doi:10.1017/S1431927622002306
Microsc. Microanal. 28 (Suppl 1), 2022
© Microscopy Society of America 2022

Comparison of Compression Methods for Ptychographic Reconstructions through Decomposition of the Diffraction Patterns in Orthonormal Bases

Anton Gladyshev[1], Marcel Schloz[1], Thomas C. Pekin[1] and Christoph T. Koch[1*]

[1.] Humboldt-Universität zu Berlin, Institut für Physik & IRIS Adlershof, Berlin, Germany.
* Corresponding author: christoph.koch@hu-berlin.de

Ptychography [1,2,3] is a computational imaging technique which uses four-dimensional scanning transmission electron microscopy (4D-STEM) datasets containing diffraction patterns recorded with a pixelated detector at various scan positions. The technique can recover the object function (consisting of the electrostatic potential of the sample and an imaginary potential accounting for absorption) using various algorithms, including ones that are based upon the strong phase approximation and in some implementations can also include the multislice formalism to account for multiple scattering. The specimen structure can be recovered in the direction perpendicular to the beam propagation direction and, in case of the multislice approach, also along it. Many ptychography reconstruction algorithms, such as ROP [4], PIE [5] or ePIE [6] are iterative and in order to achieve convergence of the object function, they typically require an overlap of the specimen areas covered by the incoming probe at adjacent scan positions. The combination of partial spatial coherence of the illumination, detector size, and desired resolution of the reconstruction puts a limit on the minimum amount of acquired data and thus limits the range of other desirable experimental parameters [7,8] such as the number of sequential scans (e.g. during in situ experiments) that can be acquired, or the field of view that can be scanned. One way to overcome this constraint is compression of the diffraction patterns.

Here, we compare compression methods for ptychography using the decomposition of diffraction patterns in orthonormal bases. The dataset used was simulated using qstem [9], including thermal diffuse scattering. A 92 Å thick atomistic model of a silicon crystal containing a 60° edge dislocation dissociated into a stacking fault bounded by a 30° and 90° partial dislocation [9] was scanned by the probe at an accelerating voltage of 60 kV with a step size of 1 Å. To perform electron ptychography we reconfigured the Python package ADORYM [10], originally developed for x-ray ptychography reconstructions. The simulated detector had 500x500 pixels covering scattering angles that corresponded to a real-space sampling of 0.07 Å in both dimensions. Compression was implemented by decomposing the diffraction patterns using an orthonormal basis set, whose elements (masks) had the same dimensions as the patterns. To include the compression in the reconstruction algorithm the decomposition coefficients were calculated as Frobenius inner products of patterns with masks using a convolution layer within the PyTorch-implementation of ADORYM (**Fig. 1a**). Subsequently the coefficients of predicted and measured patterns were compared using the l^2-norm. Thus, for each diffraction pattern the amount of stored data was reduced from the total number of pixels to the number of decomposition coefficients. We found that if the probe function is initially well defined, the dark field area of the patterns could be totally neglected, and for the mismatch calculation one could use only masks covering the bright field disc. However, when simultaneously optimizing the probe and object functions, the probe diverged in the unmasked regions of the diffraction patterns. An additional set of masks covering the dark field was added, but the decomposition coefficients corresponding to these masks were strictly set to zero in order to keep a low number of knowns.

https://doi.org/10.1017/S1431927622002306 Published online by Cambridge University Press

Binning was chosen to be our initial compression algorithm (see also [4]). In our implementation, it can be computed by using square-shaped non-overlapping masks, that average the pattern value over an area. This was compared with a set of 2D Zernike polynomials (**Fig. 1b**), whose radius of the circular masks was matched to the radius of the transmitted beam, while the rest of the detector plane was covered by one donut-shaped mask.

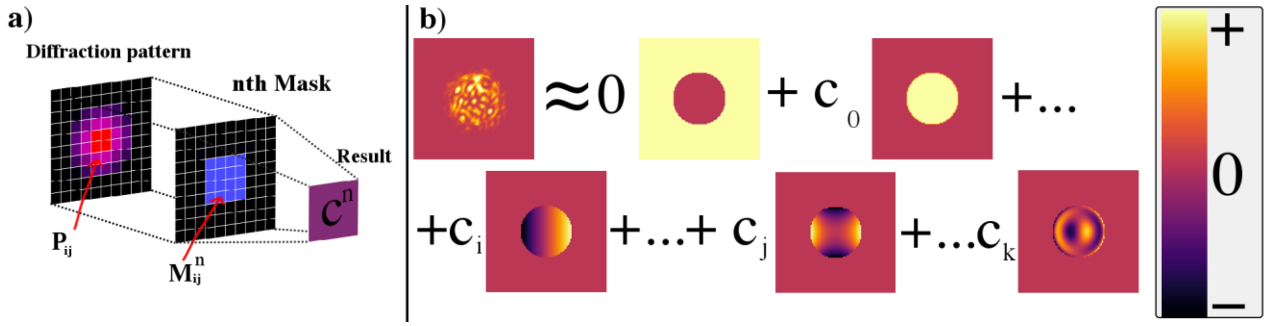

Figure 1. a) Working principle of our masking process. The diffraction pattern with elements P_{ij} is multiplied element-wise with the n^{th} mask from the chosen basis containing elements M^n_{ij},. Subsequently, the multiplication products are summed up. Using the Einstein summation convention, the result c^n is equal to $P_{ij}M^n_{ij}$,. **b)** Decomposition of a diffraction pattern using Zernike polynomials. For bright field masks the decomposition coefficients c_n are calculated using a convolution layer, for the dark field covering donut-shaped mask the coefficient is strictly set to zero.

For both of the described basis options we have tested how reducing the number of knowns affects the results of the reconstructions. **Fig. 2** demonstrates the Fourier shell correlation between reconstruction results of an uncompressed data set and reconstructions from multiple compressed data sets.

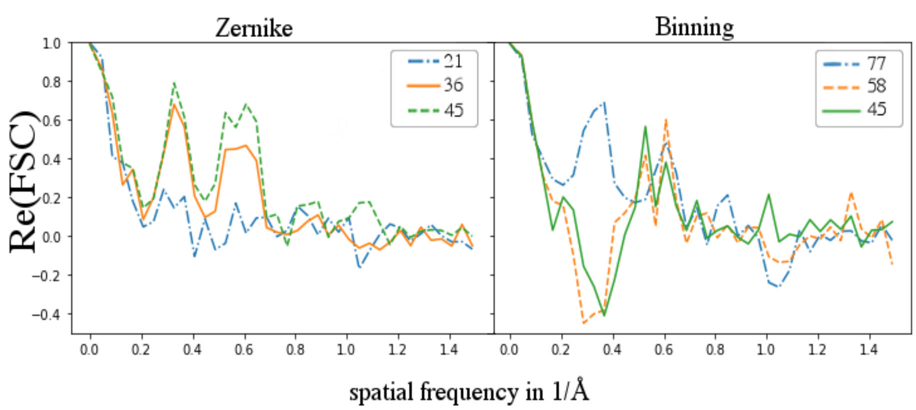

Figure 2. Real part of Fourier shell correlations (FSC) between the result of an uncompressed reconstruction and results of various compressed reconstructions, labeled with the number of stored values.

https://doi.org/10.1017/S1431927622002306 Published online by Cambridge University Press

We have found that through the use of Zernike polynomials, it is possible to compress the representation of our diffraction patterns from 2.5e5 pixels to 36 coefficients. This results in a 99.9856% decrease in necessary storage requirements. Binning required at least 45 masks, each having a size of 7 px x 7 px, covering the circular area of the BF discs and resulting a 99.982% decrease in storage requirements. **Figure 3** shows the results of these two reconstructions and a third without compression, recovering 4 different slices within the object.

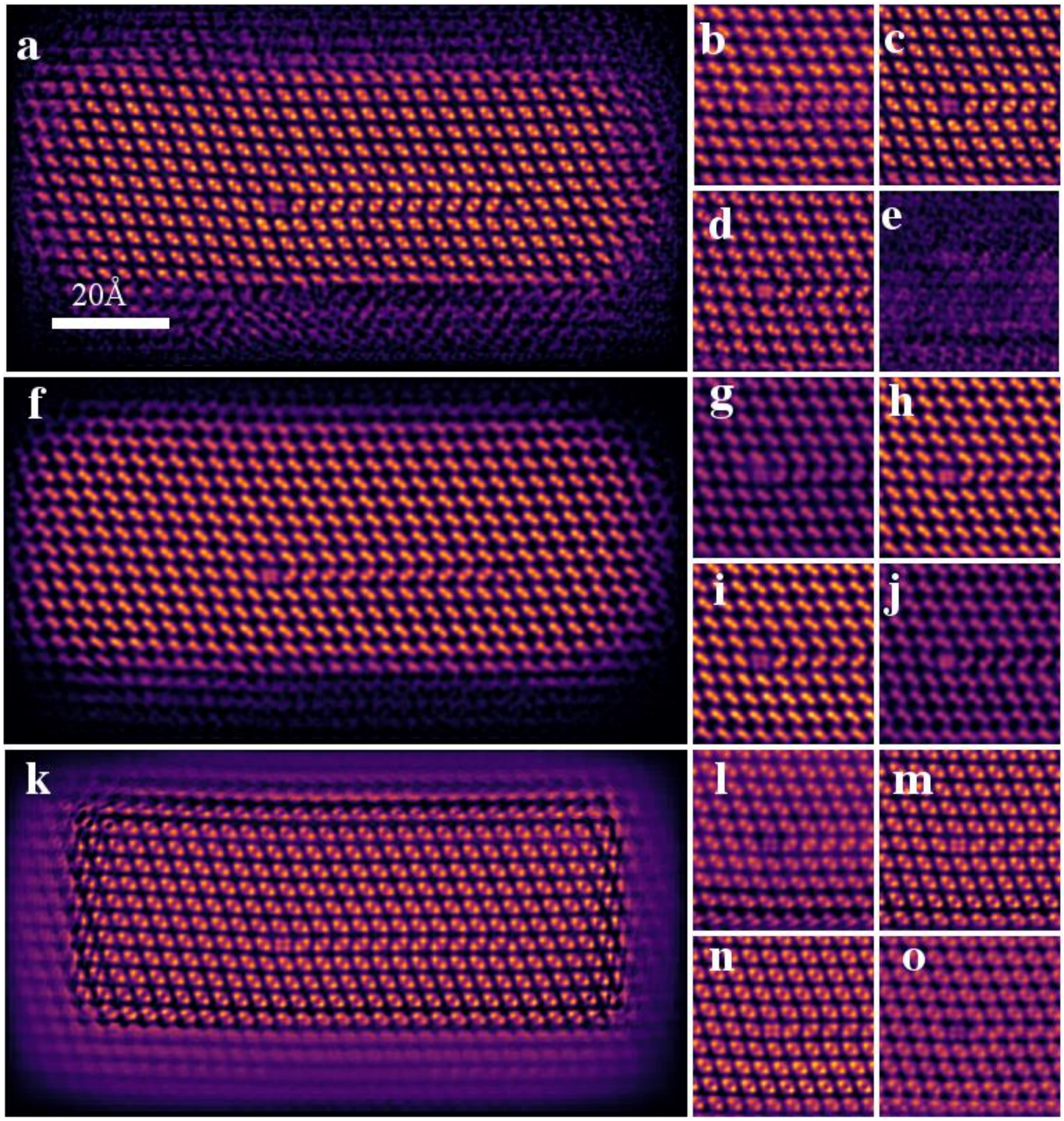

Figure 3. The second slice from a four-slice multislice reconstruction using **a)** Zernike decomposition using 36 masks, **f)** binning using 45 masks and **k)** an uncompressed reconstruction. For each

https://doi.org/10.1017/S1431927622002306 Published online by Cambridge University Press

reconstructions the slice positions along the beam were set to 0, 30.7 Å, 61.3 Å and 92 Å. Subsections of all four slices can be seen for **b-e)** Zernike compression, **g-j)** binning and **l-o)** uncompressed.

While the probe was scanned at a step size of 1A the potential was recovered at a sampling of 0.07 Å, i.e. even when reconstructing only a phase shift for a single slice, more than 200 data points per probe position would be necessary to prevent the reconstruction from being underdetermined. In the cases shown in Fig. 1 a) – j) much less data has been given into the reconstruction. As we have shown earlier [4] underdetermination of the problem can be counteracted by regularizing the solution. The constraints applied here included strict zeroing of the pixel values of the diffraction patterns in the dark field region as well as bandwidth limiting of the incident probe to the size of the condenser aperture. Finally, the number of iterations required for a reconstruction from compressed data depends on the number of masks being used. The number of bright field masks used for the compared compression methods were very close to each other, but for binning we used more dark field masks, thus requiring more time [11].

References :

[1] W Hoppe in "Acta Crystallogr." (1969). p. 409.
[2] J Rodenburg, Advances in imaging and electronphysics **150** (2008), p. 87. doi:10.1016/S1076-5670(07)00003-1
[3] P Nellist et al., Nature **374** (1995), p. 630. doi:10.1038/374630a0
[4] M Schloz et al., Optical Express **28** (2020), p. 28306. doi: 10.1364/OE.396925
[5] J Rodenburg and H Faulkner, Applied Physics Letters **85** (2004), p. 4795. doi:10.1063/1.1823034
[6] A Maiden and J Rodenburg, Ultramicroscopy **109** (2009), p. 1256. doi: 10.1016/j.ultramic.2009.05.012
[7] P Li and A Maiden, Scientific Reports **8** (2018), p. 2049. doi: 10.1038/s41598-018-20530-x
[8] C O'Leary et al., Microsc. Microanal. (2021), p. 1. doi:10.1017/S1431927621012587
[9] C Koch, PhD thesis, Arizona State University (2002).
[10] M Du et al. Optical Express **29** (2021), p. 10000. doi: 10.1364/OE.418296
[11] The authors acknowledge financial support through the DFG (SFB 951 and SFB 1404).

https://doi.org/10.1017/S1431927622002306 Published online by Cambridge University Press